Defence Science Journal, Vol. 74, No. 3, May 2024, pp. 305-315, DOI : 10.14429/dsj.74.19902

High Strain Rate Modeling of CFRP Composite Under Compressive Loading

Bipin Kumar Chaurasia and Deepak Kumar*

Department of Mechanical Engineering, National Institute of Technology, Jamshedpur - 831 014, India
**E-mail: deepak.me@nitjsr.ac.in*

ABSTRACT

An in-depth understanding of how Carbon Fiber-Reinforced Plastics (CFRP) respond to intense strain rates is essential, particularly in non-linear deformation and dynamic loading situations. The authors performed a computational study to examine the behavior of CFRP composites when exposed to high strain rates under compressive loading. Specifically, we employed Split Hopkinson Pressure Bar models for cohesive interfacial simulations, continuum shell analysis, and laminated composites oriented at 0° at a strain rate equivalent to 900 s^{-1}. The Finite Element model utilized a custom Hashin damage model and a Vectorized User Material (VUMAT) sub-routine to identify degradation damage within the CFRP composite model. The quasi-isotropic composite demonstrated a significant enhancement in dynamic strength compared to static values, attributed to its intense sensitivity to strain. As confirmed by experimental test results, numerical simulations accurately predicted stress (σ)-strain (ε) and strain rate ($\dot{\varepsilon}$) curves. Additionally, it was observed that the relationship between damage behavior varied depending on the element type used.

Keywords: CFRP; High strain rate; Hashin failure; VUMAT

1. INTRODUCTION

Carbon fiber laminates are widely employed in defense and aerospace sectors, where they frequently experience dynamic loading conditions such as ballistic impacts and high-velocity collisions. These scenarios often lead to rapid strain rate deformation[1]. Traditionally, experimental methods have been used to determine the compressive strength of these materials. However, an alternative approach is to estimate the compressive strengths of unidirectional fiber-reinforced composites using constitutive laws and fiber micro-buckling models. During high-strain rate deformations, localized damage occurs around contact sites, which results in energy dissipation[2]. Given that strain-rate effects significantly impact carbon-fiber-reinforced polymer failure mechanisms; it becomes crucial to accurately predict the behavior of these materials under impact loading conditions before their application in various industries.

Gavrus[3], *et al.* conducted experiments using the Split Hopkinson Pressure Bar technique to investigate high strain rates in Aluminium alloy specimens. In addition, they simulated these experiments using Finite Element (FE) software by incorporating the deformation behavior of orthotropic and isometric alloys. This approach allowed for a study of the relationship between strain rate and time. Lu, *et al.*, on the other hand, carried out a related experiment utilizing the Johnson-Cook metal damage model along with the user-defined material (UMAT) subroutine[4]. Furthermore, Ls-dyna has been used in research simulations employing an elastic-plastic model to predict specific damages in SHPB test configurations[5-7]. Some researchers have used the Johnson-Cook damage model in composite materials but have not considered any defects within fibers or matrices during their studies[8-9].

In addition, researchers have utilized various criteria to assess the failure of Fibre Reinforced Plastics (FRP) in predicting high-strain rate models[10-11]. These criteria provide suitable measures for unidirectional plies and laminates that undergo in-plane stresses at low and moderate strain rates[12-13]. The 3-dimensional (3D) Hashin criterion has been widely used to determine FRP failure criteria because of its accuracy, ease of use, and computational efficiency[14].

This study utilises a Split Hopkinson Pressure Bar configuration to simulate the specimen between the incident and transmitted bars. Hashin damage model and material degradation approach examine a non-linear, rate-dependent constitutive composite model for predicting damages. The carbon fiber stacking sequences $[0°/45°/90°/-45°]_{2s}$ with a lamina thickness of 0.3125 mm are utilized in cohesive interfaced solid models, continuum shell models, and solid models where fibers are oriented at 0°. In specimens with a 0° fiber orientation, layers have no cohesion contact as they form one unitary entity. Nonetheless, transverse shear stiffness does exist between layers in quasi-isotropic CFRP composites. The authors analyzed three different models, and their stress-strain behavior was examined and compared.

2. NUMERICAL DAMAGE MODEL

The CFRP composite employs the Hashin damage model within a user-defined Vectorized User Material (VUMAT) subroutine. The Orthotropy of the CFRP composite serves as

Received : 12 February 2024, Revised : 08 March 2024
Accepted : 11 March 2024, Online published : 10 May 2024

the foundation for establishing criteria for initiating damage based on the principles of Hashin's damage theory[15]. This comprehensive theory encompasses four failure modes: compression and tension in matrix and fiber components. Utilizing this model incorporates a law that considers both fiber and matrix failures when assessing damage initiation. This approach allows for a more realistic and accurate representation of CFRP composites' mechanical behavior and failure characteristics in simulation models. By incorporating the Hashin damage model into the simulation models of CFRP composites, a more accurate prediction of failure modes and initiation can be achieved. The following Eqn.s (1-5) were considered for the damage initiation.

Fiber tensile failure

$$F_{ft} = \left(\frac{\sigma_1}{X_t}\right)^2 + \left(\frac{\sigma_{12}}{S_{12}}\right)^2 + \left(\frac{\sigma_{13}}{S_{13}}\right)^2 \geq 1 \quad (1)$$

Fiber compressive failure

$$F_{fc} = -\left(\frac{\sigma_1}{X_c}\right) \geq 1 \quad (2)$$

Matrix tensile failure ($\sigma_{22} + \sigma_{33} \geq 0$)

$$F_{mt} = \left(\frac{\sigma_2}{Y_t}\right)^2 + \left(\frac{\sigma_{23}}{S_{23}}\right)^2 + \left(\frac{\sigma_{12}}{S_{12}}\right)^2 + \left(\frac{\sigma_{13}}{S_{13}}\right)^2 \geq 1 \quad (3)$$

Matrix compressive failure ($\sigma_{22} + \sigma_{33} < 0$)

$$F_{mc} = \left(\frac{\sigma_2}{2S_{23}}\right)^2 + \left(\frac{\sigma_2}{Y_c}\right)\left[\left(\frac{Y_c}{2S_{23}}\right)^2 - 1\right] + \left(\frac{\sigma_{12}}{S_{12}}\right)^2 + \left(\frac{\sigma_{23}}{S_{23}}\right)^2 \geq 1 \quad (4)$$

Shear failure

$$F_S = \left(\frac{\sigma_1}{X_c}\right)^2 + \left(\frac{\sigma_{12}}{S_{12}}\right)^2 + \left(\frac{\sigma_{23}}{S_{13}}\right)^2 \geq 1 \quad (5)$$

In the above expressions, σ_{ij} represent the stress tensor components, X_t and X_c are tensile and compressive strength in the fiber direction. Y_t and Y_c represent tensile and compressive strength in the transverse direction. S_{12}, S_{13}, S_{23} are shear strength in the respective direction. If any of the failure values reaches 1, then the damage initiates ($\sigma=\sigma_0$), and after that, damage evolves.

Furthermore, damage caused by material property degradation starts in the composite specimen. The damage model with a gradual degradation scheme is applied for this damage evolution. The equation for the damage criterion is given as follows (Eqn. (6)):

$$d_I = \frac{\delta_{1,eq}^f\left(\delta_{1,eq} - \delta_{1,eq}^0\right)}{\delta_{1,eq}\left(\delta_{1,eq}^f - \delta_{1,eq}^0\right)} \rightarrow (d_I \in [0,1], I = ft, fc, mt, mc, s) \quad (6)$$

Here, $\delta_{1,eq}^0$ represents the displacement of damage initiation and $\delta_{1,eq}^f$ is for final failure displacement and $\delta_{1,eq}$ are equivalent displacements corresponding to obtained stresses.

The simulation incorporated the numerical damage model by following the flow diagram of the material damage model (Fig. 1). The initial input parameter and boundary condition were utilized, and a restricted number of load increments and checks for damage initiation were completed. It is presumed that the material exhibits perfect elasticity during its early linear elastic phase (i.e., before damage onset), which implies that it returns entirely to its original shape when applied forces are removed. This assumption holds under the condition that only minimal deformations occur by generalized Hook's law.

$$\sigma = C : \sigma^0$$

And the stress update in each small interval of time is given as:

$$\sigma_t = \sigma_{t-\Delta t} + C : \Delta E$$

The elastic tensor 'C' calculates the damage initiation, starting with a value less than one (<1). The process continues until the damage initiation reaches a value of one (=1). The authors examined its damage parameter to confirm if the

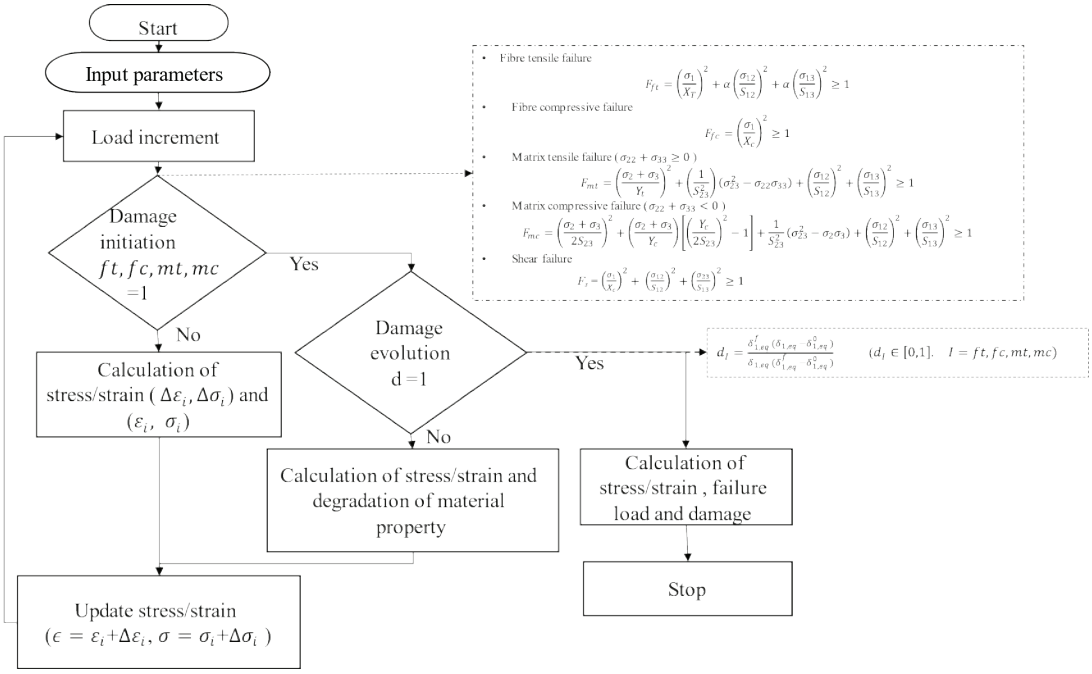

Figure 1. Flow diagram of the numerical damage model.

composite had failed. If the value of this parameter is less than 1 (d < 1), it indicates that the composite has not fallen. Therefore, they calculated properties such as stress/strain and degradation since the start of damage. After updating these properties, each load increment undergoes another cycle. The composite fails when the damage reaches a value of one (=1); at this point, further analysis can determine factors like ultimate stress/strain, failure load, and type of damage. The authors utilized the elastic tensor 'C' to determine the initiation of damage, which initially has a value of less than one (<1).

3. METHODOLOGY

Carbon fiber composite laminates were fabricated using LY556 epoxy resin, HY 951 hardener, and Unidirectional and woven carbon fabrics. The stacking sequence of the carbon fiber fabric is taken as $[0°/45°/90°/-45°]_{2s}$. LY556 epoxy resin was mix with hardener HY951 in a 10:1[20] ratio to develop the resin solution. After manufacturing, we have removed the composite and cut the specimen following ASTM D7136 testing requirements (Fig. 2) using High Strength Steel (HSS) and carbide-tipped tools[16].

Figure 2. CFRP composite test specimens

The experimental process utilizes the SHPB test set-up. Figure 3 shows the SHPB test set-up designed for stress reversal testing. The critical components of the set-up consist of Hopkinson bars made of marage steel, namely the striker (0.15 m), incident bar (1.4 m), and transmission bars (1.4 m length) with a 12 mm diameter. These parts include a barrel resembling a gun, a hitting mechanism, and a recording device. A strain gauge is also installed to monitor the strain rate using transmitted bar data.

4. SHPB 1-DIMENSIONAL WAVE

The Split Hopkinson Pressure Bar test utilizes longer incident, transmitted, and striker bars than the specimen's thickness. This allows for a simplified one-dimensional wave equation approach with limited consideration of other factors. Thus, the change in displacement over time within the specimen was measured as follows (Eqn. 7-8): [17]

$$\dot{u}_1 = \frac{\delta u_1}{\delta t} = -f^{'}.C_{OB} + g^{'}.C_{OB} = C_{OB}\left(g^{'} - f^{'}\right) = C_{OB}\left(\varepsilon_R - \varepsilon_I\right) \quad (7)$$

$$\dot{u}_2 = \frac{\delta u_2}{\delta t} = -C_{OB}\left(\varepsilon_T\right) \quad (8)$$

From that, the average strain rate is expressed as (Eqn. (9)):

$$\varepsilon_s = \frac{u_1 - u_2}{L_s} = \frac{C_0}{L_s}\int_0^t \left(\varepsilon_I - \varepsilon_R - \varepsilon_T\right)dt = 2\frac{C_0}{L_s}\int_0^t \left(\varepsilon_R\right)dt \quad (9)$$

After considering force equilibrium, $\varepsilon_I + \varepsilon_R = \varepsilon_T$ (10)

Strain rate $(\dot{\varepsilon})$ can be calculated by using Eqn. (9) and Eqn. (10) as (Eqn. (11)):

$$\dot{\varepsilon} = \frac{C_0\left(\varepsilon_I - \varepsilon_R - \varepsilon_T\right)}{L_s} = \frac{2\varepsilon_R C_0}{L_s} \quad (11)$$

Here, $\dot{u}_1$ and $\dot{u}_2$ represent the change in displacement with respect to time, C_O is the sound velocity, L_s represent the specimen's instantaneous length, ε_I , ε_R and ε_T represent strain obtained from strain gauge in case of an incident, reflected, and transmitted wave.

5. COMPRESSIVE SHPB MODEL

5.1 CFRP Specimens

All layers of CFRP laminate are designed with a unique fiber direction, with a lamina thickness of 0.3125 mm and a diameter of 6 mm. The laminated composite consists of 16 layers assembled without any sliding contact, resulting in a total thickness of 5 mm. In the FE analysis, CFRP laminate is carefully modeled to separate the transmission and incident bars. The laminates with stacking sequence $[0°/45°/90°/-45°]_{2s}$ were modeled as a continuum shell model and solid model, as shown in Fig. 4.

The finite element modeling employed the Split Hopkinson Pressure Bar configuration and applied equivalent boundary conditions. Figure 5 displays the schematic model, consisting of a striker bar, the incident bar, and the transmitted bar with a diameter of 12 mm each. The dimensions included lengths of 250 mm for the striker bar and 1400 mm for both the incident and transmitted bars. In this set-up, an initial velocity of 108 m/s was imparted to the striker bar to strike against

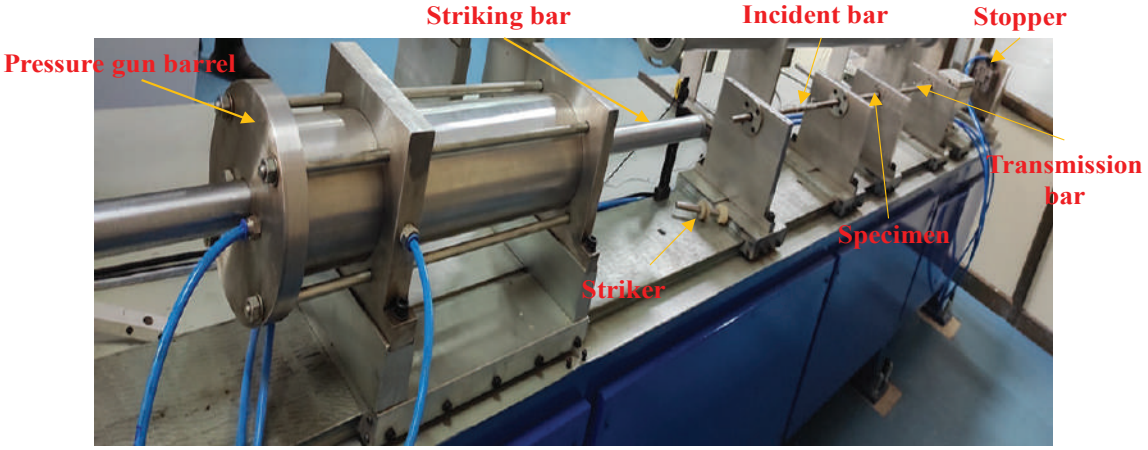

Figure 3. SHPB test set-up for compressive high strain rate testing.

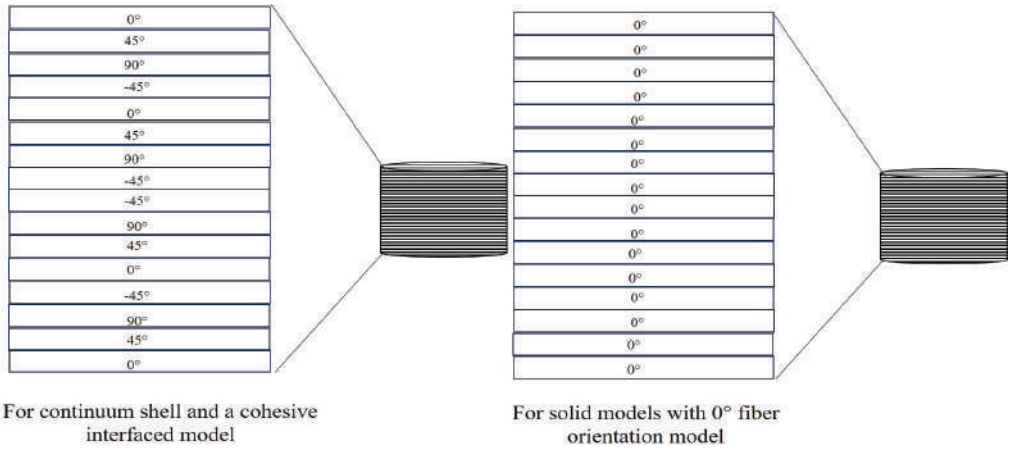

Figure 4. Fiber orientation in the composite specimen.

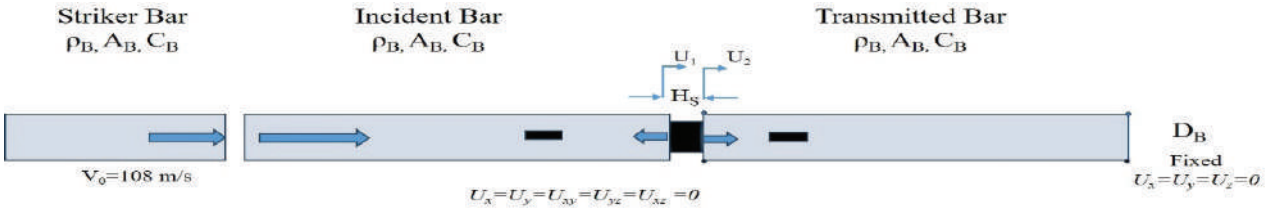

Figure 5. SHPB model.

the incident bar. Subsequently, the load was transferred from the incident bar to the specimen through the fixed damping system integrated within the transmitted bar to dissipate energy effectively. Consequently, there were notable strain rate deformations perceived within the specimen.

The model assumes that the striker is positioned 0.01 mm from the incident bar, and both bars directly contact the specimen surface—the contact between each part of the assembly by the surface-to-surface contact. The interaction between layers in the laminated composite and between bars is assumed to be hard contact. The model's boundary conditions include restricted constraint displacement motions in y and z dimensions and rotational moments in all directions (U_x=U_y=U_{xy}=U_{yz}=U_{xz}). The initial velocity of the striker is 108 m/sec. Additionally, support is provided at the end of the transmission bar (U_x=U_y=U_z). All three components - striker, incident bar, transmitted bar - are deformable solids with maraging steel properties, according to Table 1. The model considers the specific position and contact between the striker, bars, and specimen surface.

In contrast, Table 2 lists the user-defined material property for CFRP. The properties of the CFRP composite material are derived from tensile, compressive, and shear testing using a UTM machine. Additionally, it is assumed that the mechanical behavior in the Y direction is equivalent to that in the Z direction.

Table 1. Material properties of maraging steel

Density (ρ, ton/mm^3)	Young's modulus (E, *GPa*)	Poisson's ratio (υ)
8×10^{-9}	210	0.3

The model is composed of the striker, an incident, and transmitted bars meshed using C3D8R elements (Fig. 6). These mesh elements are classified as 8-node linear bricks with reduced integration and hourglass control. The cohesive interface set at a 0° orientation also uses similar meshing techniques in its respective model. Additionally, SC8R elements are incorporated into the continuum shell model featuring 8-node quadrilaterals with in-plane general-purpose continuum shells equipped with reduced integration and hourglass control capabilities alongside finite membrane strains. To ensure appropriate boundary conditions, displacement is applied in both the x and y directions, while rotational moment is considered across all axes. Additionally, an initial velocity of 108 m/s is assigned to the striker component. Stability is provided by a fixed support mechanism at the end of the transmission bar. A sensitivity analysis was carried out to evaluate finite element results stability and determine the optimal mesh element size for obtaining stabilized stress values (as depicted in Fig. 7). All simulations were performed using a finite element model consisting of 100000 elements.

Table 2. Material properties of CFRP composite

Young's modulus in the x-direction (E_1)	10.539 (*GPa*)
Young's modulus in the y=z-direction (E_2= E_3)	2.773 (*GPa*)
Poisson's ratio (v_{12})	0.27
Poisson's ratio (v_{13}= v_{23})	0.07
Shear modulus (G_{12}= G_{13})	4180 (*MPa*)
Shear modulus (G_{23})	4180 (*MPa*)
Ultimate tensile stress in the *x*-direction	619.88 (*MPa*)
Ultimate tensile stress in *y* = *z*-direction	180.277 (*MPa*)
Ultimate comp. stress in *x*-direction	231.88 (MPa)
Ultimate comp. stress in *y* = *z*-direction	34 (MPa)
Ultimate shear stress (S_{12} = S_{13})	112.83 (MPa)
Ultimate shear stress (S_{23})	23.18 (MPa)

Figure 6. Meshed model.

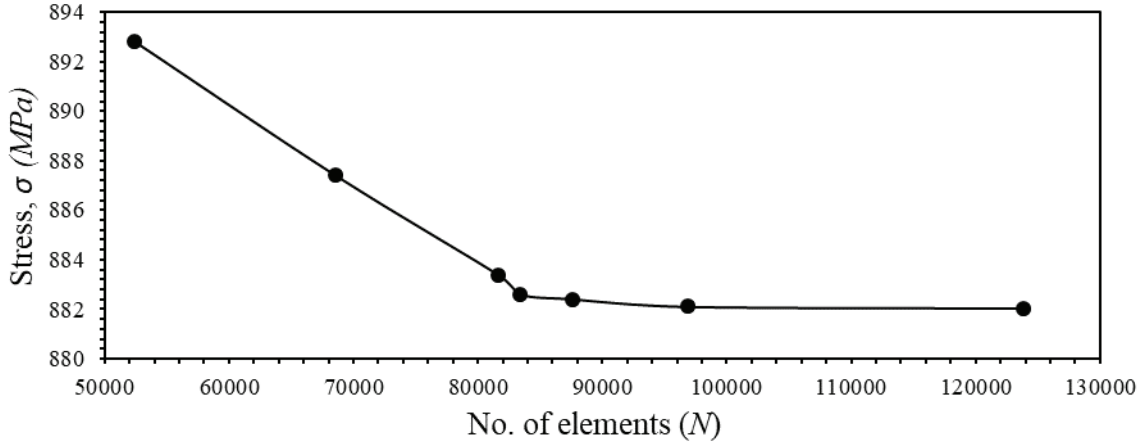

Figure 7. Mesh sensitivity analysis for SHPB set-up.

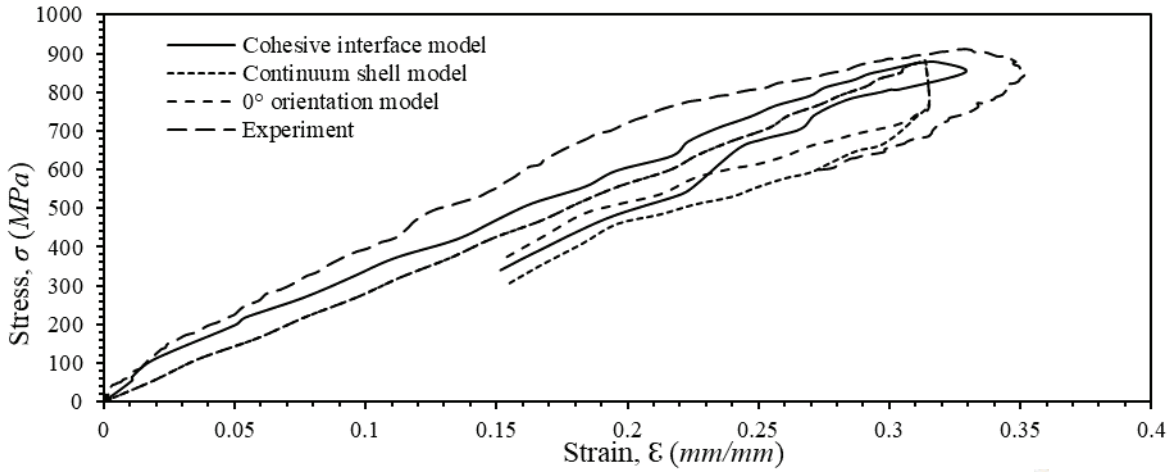

Figure 8. Stress (σ) vs strain (ε) plot for CFRP composite under 900 s-1 strain rate ($\dot{\varepsilon}$).

6. RESULTS AND DISCUSSION

The SHPB test method was used to apply stress to CFRP composite specimens by impacting them with an incident bar and applying compressive force. This results in the development of strain in the specimens. The specimen's behavior was analyzed through a stress (σ)-strain (ε) plot, comparing similar simulation data for the cohesive interface, continuum shell, and 0° orientation models. These stresses were measured in the incident bar.

A comparison between the three stresses (σ)-strain (ε) models shows a similar trend with experiments. The numerical model, illustrated in the graph, exhibits a stress-strain pattern with a minor variation from the investigation. These variations of stress in the specimen are due to voids and interface characteristics of the experiment. Compared to the other two damage models, the cohesive interfaced model exhibits more comparable stress-strain graph trends because of the cohesive interface. In the case of a cohesive interfaced model, there is an error of 2.54 % at the critical stress. The stress and strain behavior in the continuum shell model and the orientation at 0° fiber laminate display a similarity before failure initiation. However, noticeable differences occur regarding changes in stress values due to material damage. Specifically, there is a significant decrease in stress value within the continuum shell model compared to that seen in the solid model with zero-degree orientation. For each case analyzed, it was found that experimentally obtained values for maximum strength deviate by approximately 2.98 %.

Figure 9 (a-f) demonstrates the development of stress over time in the continuum shell model of the CFRP composite. In Figure 9(a), stress is observed to initiate on the surface of the composite laminate immediately after contact between the incident bar and composite specimen at a time interval of 0.25 μs. Subsequently, this stress propagates throughout the entire body of the CFRP composite specimen, as shown in Fig. 9(c), at a time interval of 1 μs. Afterward, there is an outward movement of both bars away from each other towards their respective surfaces where they made contact initially. The evolution of the cohesive interface model over time can be observed in Fig. 10 (a-f). Implementing a cohesive interface in the three-dimensional model allows for a more accurate stress distribution within the composite lamina. Initially, stress is generated at the interface between the incident bar and

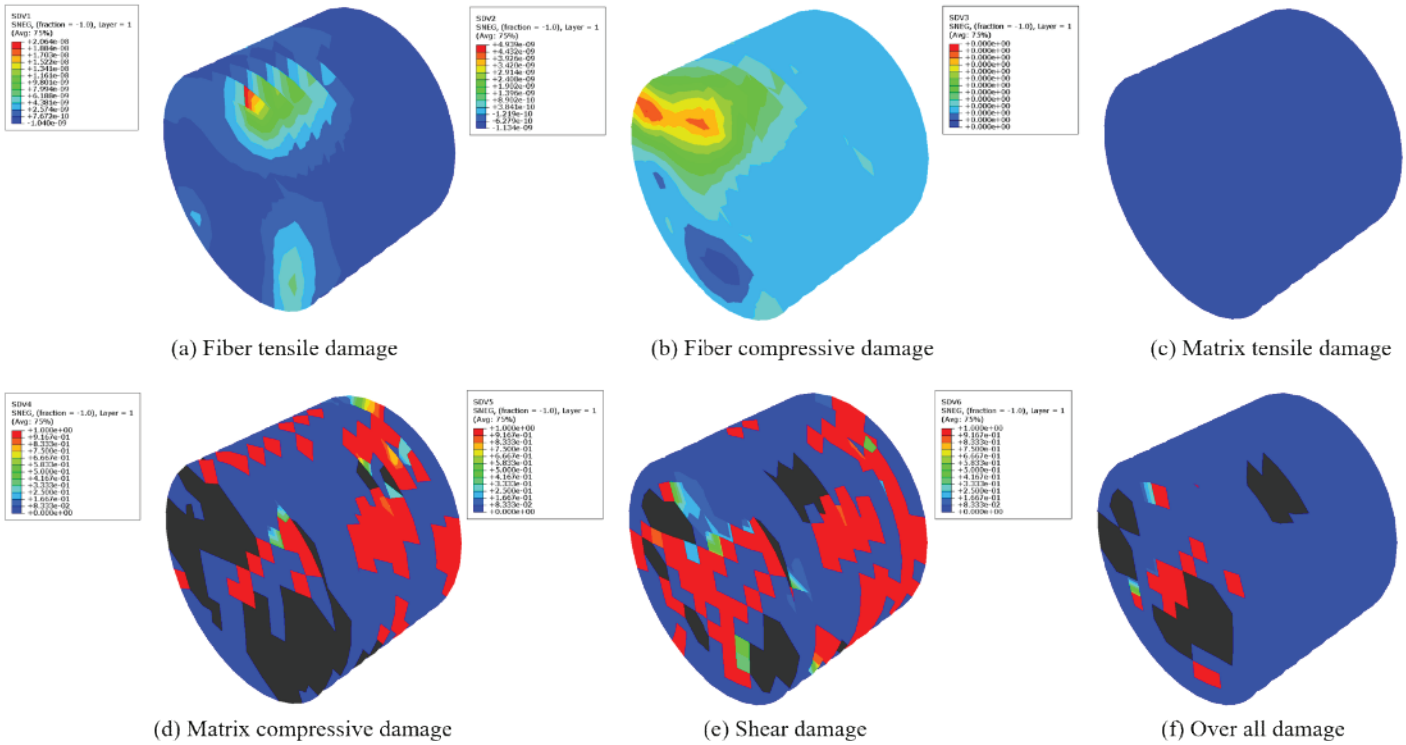

Figure 9. Stress variation in the continuum shell model at (a) 0.25 µs, (b) 0.5 µs, (c) 1 µs, (d) 1.5 µs, (e) 2 µs and (f) 2.25 µs.

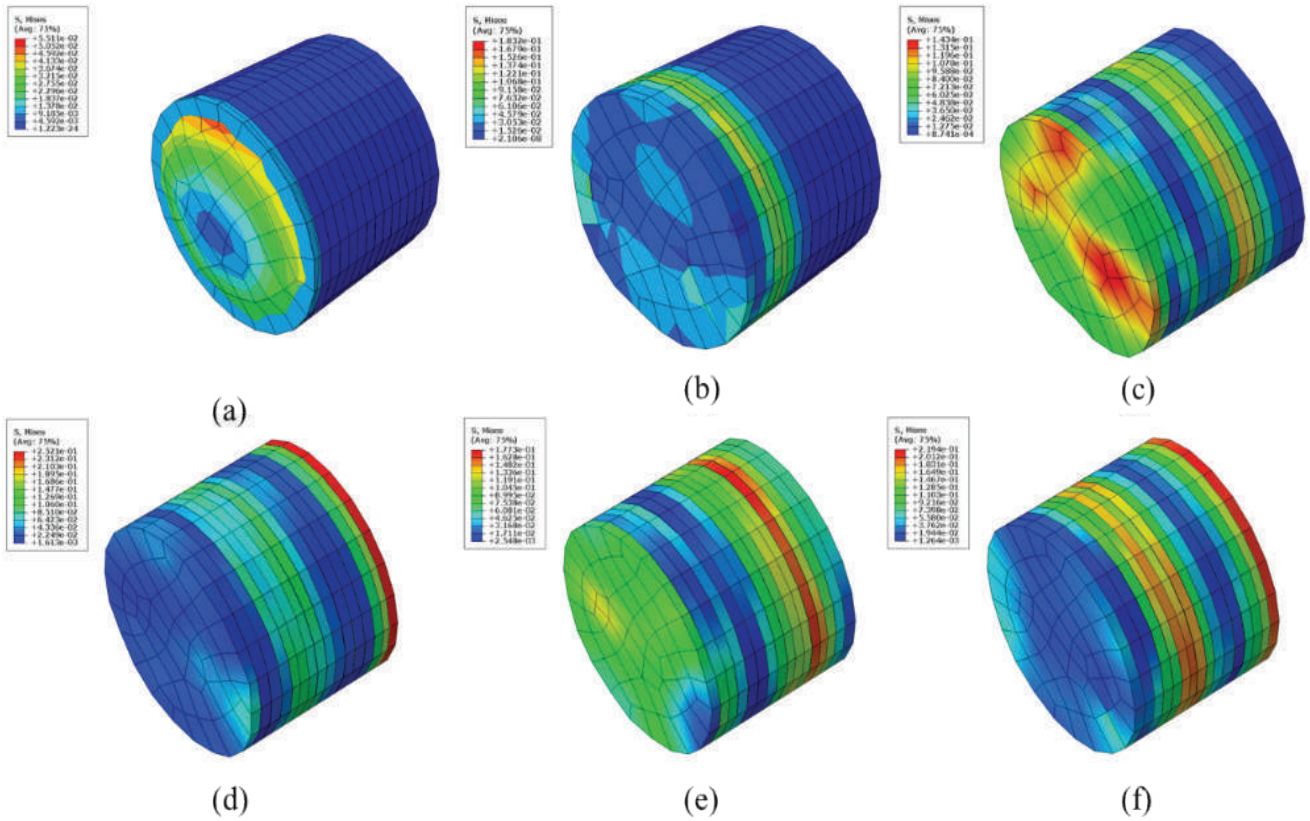

Figure 10. Stress (σ) variations in the cohesive interface model at (a) 0.25 µs, (b) 0.5 µs, (c) 1 µs, (d) 1.5 µs (e) 2 µs and (f) 2.25 µs.

specimen, spreading throughout the specimen. Throughout this process, there are variations in stress levels within different parts of the composite model. However, it is notable that critical stress occurs only at 0° and 90° ply orientation. This emphasizes how significantly the cohesive interface influences composite materials' overall stress distribution and behavior.

Figure 11 (a-f) illustrates the composite specimen's stress distribution throughout 2.25 µs. In this CFRP composite with a fiber orientation of 0°, the stress distribution is initially

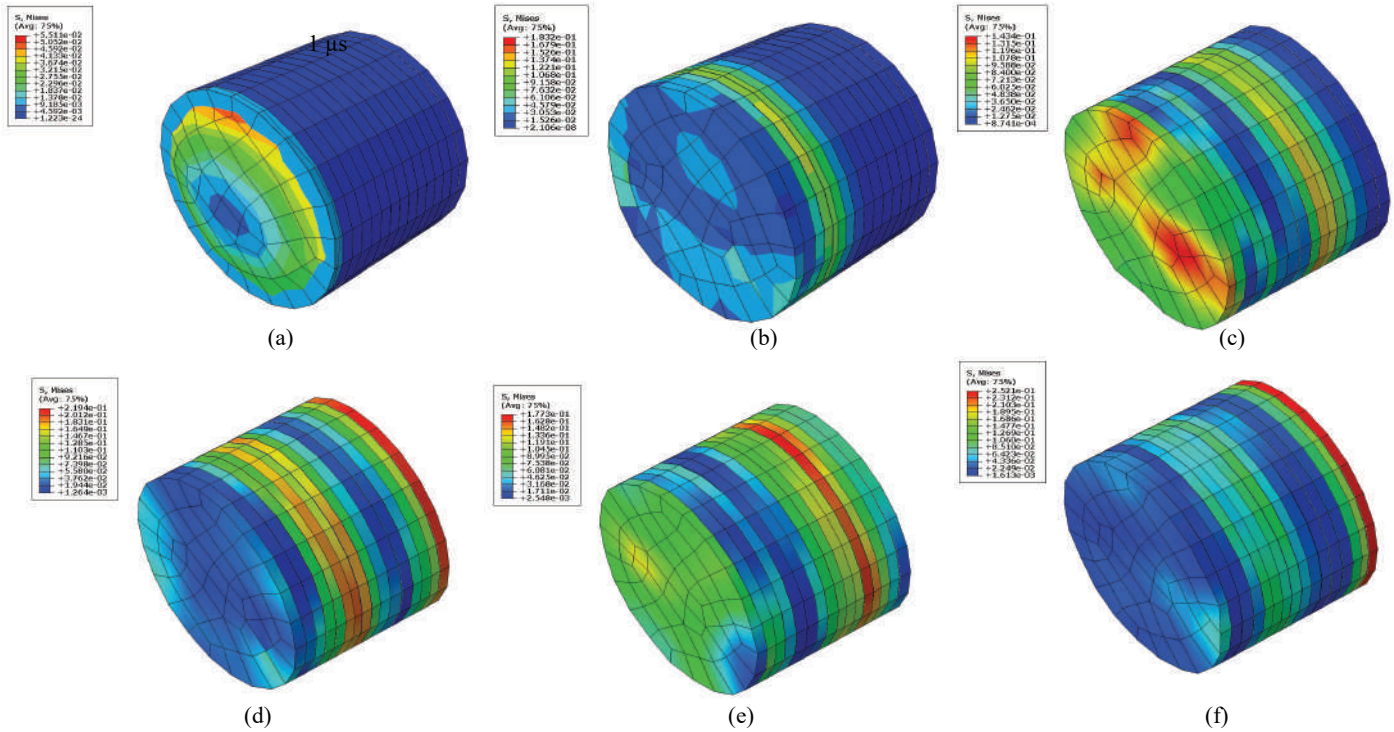

Figure 11. Stress (σ) variations in solid models with 0° fiber orientation at (a) 0.25 µs, (b) 0.5 µs, (c) 1 µs, (d) 1.5 µs (e) 2 µs and (f) 2.25 µs.

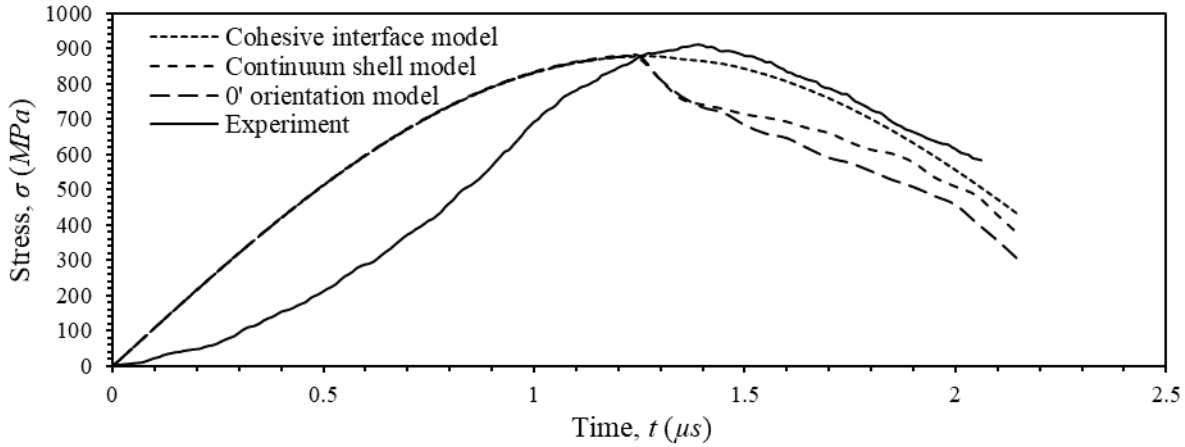

Figure 12. Stress (σ) vs time (t) plot for CFRP composite.

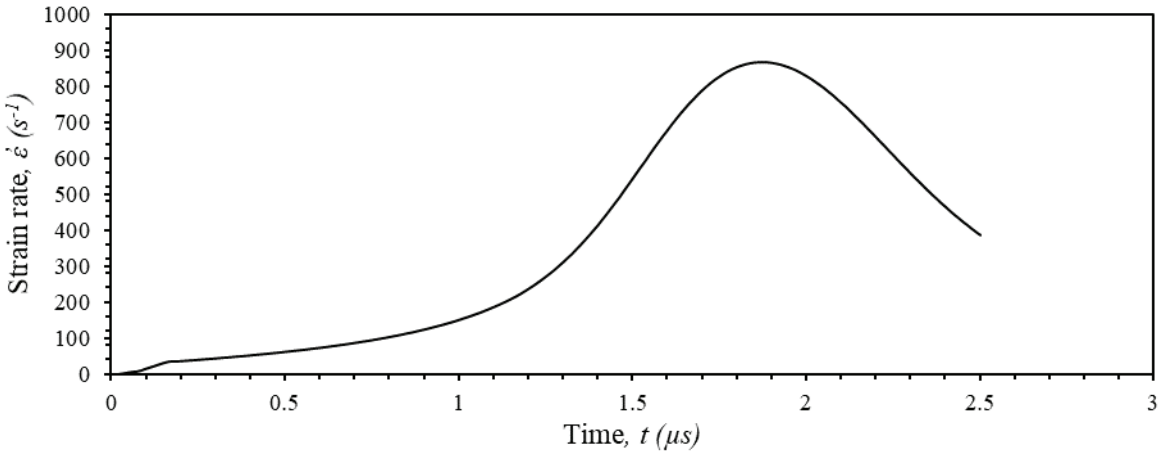

Figure 13. Strain rate ($\dot{\varepsilon}$) plot for CFRP composite cohesive interface model.

similar to the cohesive interface model. However, as the stress reaches its critical value, it spreads throughout the entire body, as depicted in Figure 11 (d), and propagates towards one end (Fig. 11(f)). In this case, wave propagation influences stress concentration rather than fiber orientation.

The stress behavior over time is shown in Fig. 12 for all three finite element models and the experimental results. It can be observed that there is a slight variation in stress values across the models until damage starts to occur, but after that point, there is a significant change in stress values. Furthermore, it should be noted that the cohesive interface model demonstrates behavior that is more similar to the experimental findings. Figure 13 illustrates how strain rate changes with respect to CFRP composite material when subject to impact on the incident bar. The SHPB test set-up and Eqn. (7-11) derived from the one-dimensional wave equation imply that the strain rate remains independent of specimen type and relies solely on characteristics of the incident bar. The highest strain rate occurs at approximately 2 μs, where both experimentally collected data and analytically modeled data show a consistent value of roughly 900 /s.

Figure 13 illustrates the strain rate behavior of the CFRP composite. The impact on the incident bar directly influences an increase in strain rate, as shown in the plot (Fig. 13). In the SHPB test set-up, the strain rate is determined by the incident bar and remains constant across different specimen types, following a 1-D wave equation (Eqn. 7-11). The maximum observed strain rate occurred at two microseconds (μs), with the FE model and experimental evaluation yielding a value of 900/s for this peak strain rate.

Figure 14 (a-f) demonstrates the continuum shell model, which showcases various types of damage in composites, such as tensile and compressive matrix damage, shear damage, and overall damage. According to this model, shear damage results in the most significant destruction compared to other damages. On the other hand, the impact of the tensile matrix is minimal. Both compressive matrix and general cumulative loss also lead to critical levels where failure occurs. The continuum shell model provides a comprehensive understanding of different forms of damage in composites. The continuum shell model allows researchers to analyze and predict various types of damage in composites, including fiber, matrix, and shear.

Figure 15 (a-f) shows the damages observed in solid models with a fiber orientation angle of 0°. The distribution of these damages is mainly influenced by the stress rather than the fiber's direction. A consistent pattern can be seen across the specimen's damage parameter, where shear matrix and fiber compression reach critical failure values. Within composite specimens, approximately 11% accounts for damaged fibers and 9 % for matrix compressive damage, respectively. Additionally, about 18 % shear damage is predicted in the solid model.

Figure 16 (a-f) presents a visual representation of different types of damage observed in the cohesive interface of the 3-D solid model. These include tension-related damages in fibers and matrices and compression, shear, and overall damage. Surprisingly, failure in the composite material is primarily attributed to compressive and shear failures within the specimen rather than failure caused by exceeding critical points for tensile damages in fibers or matrices. Approximately 19 % of elements reach their crucial point for compressive fiber failure, while it is about 13 % for compressive matrix failure. The highest level of damage occurs from shear stress, with around 24 % of elements surpassing their critical.

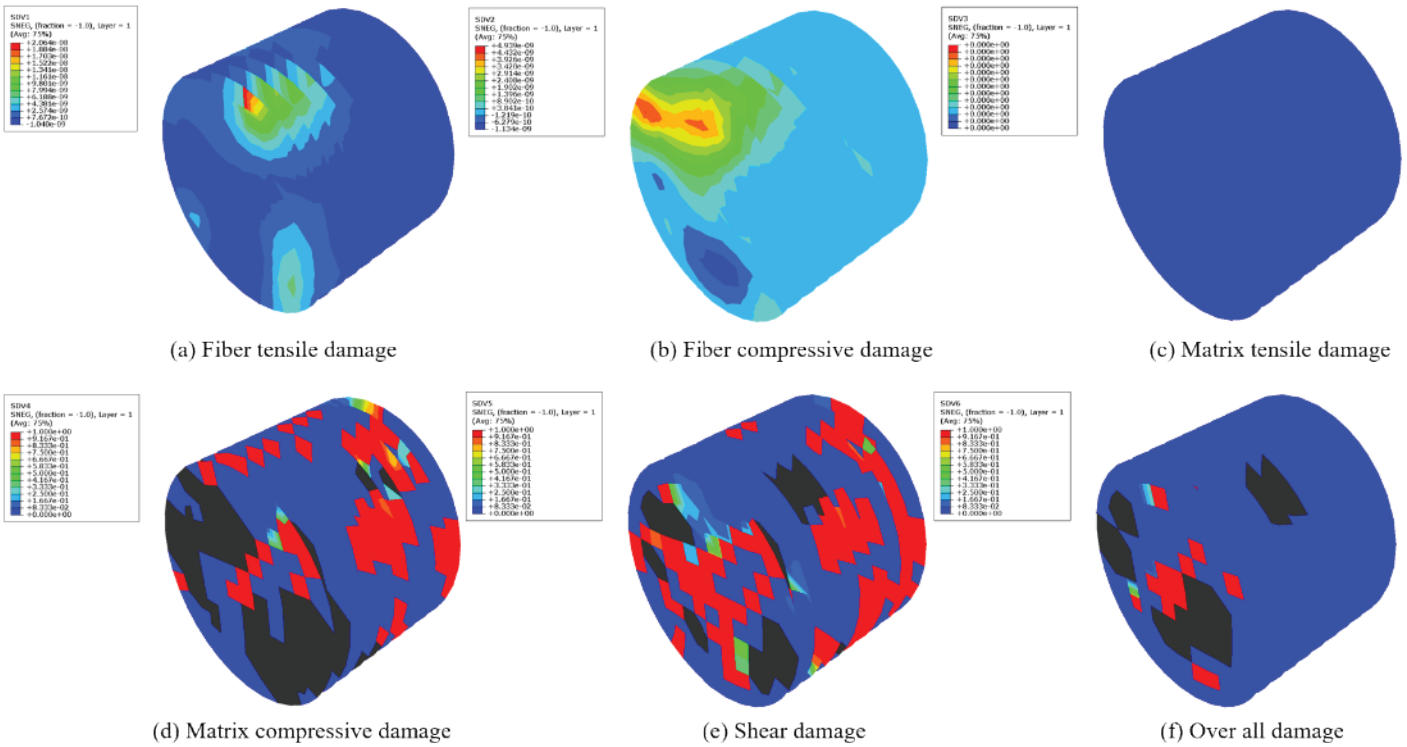

(a) Fiber tensile damage (b) Fiber compressive damage (c) Matrix tensile damage

(d) Matrix compressive damage (e) Shear damage (f) Over all damage

Figure 14. Damages obtained for the continuum shell model.

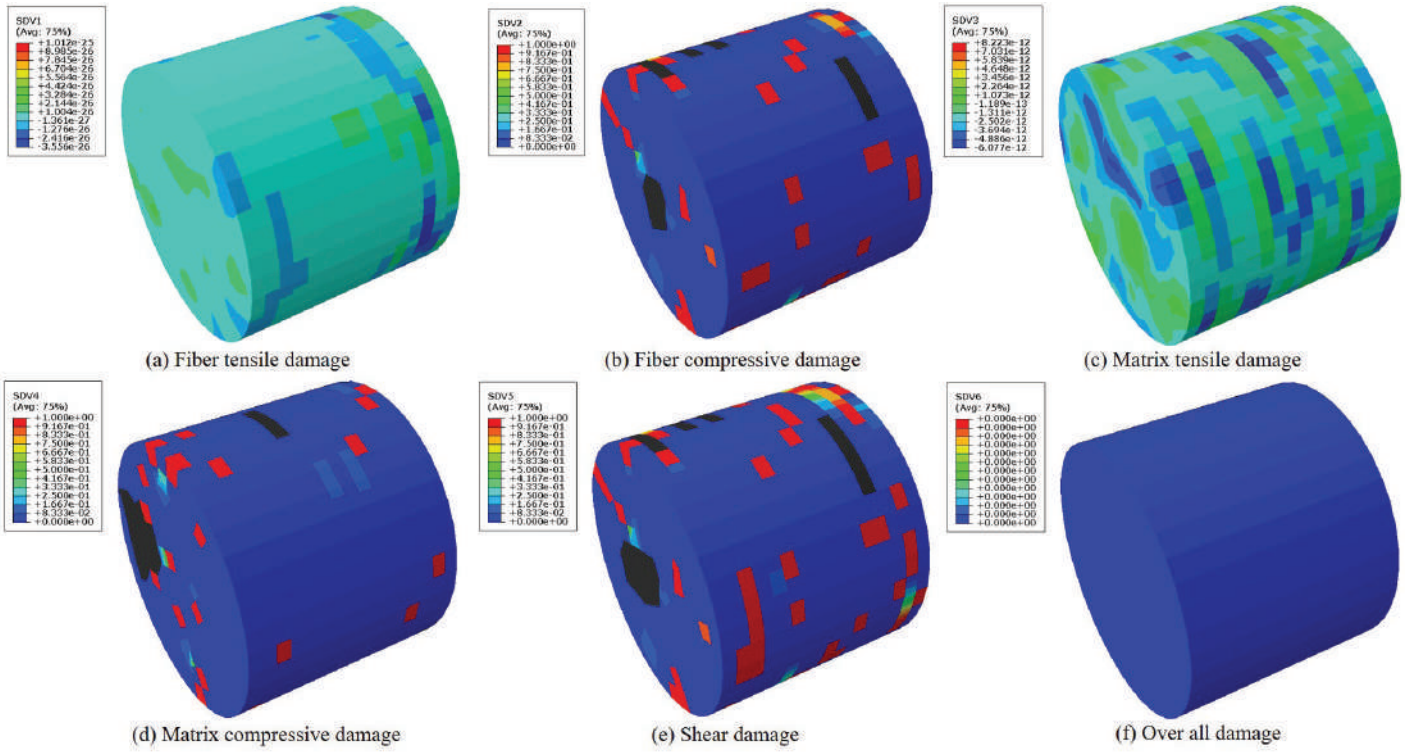

Figure 15. Damages obtained for solid models with 0° fiber orientation.

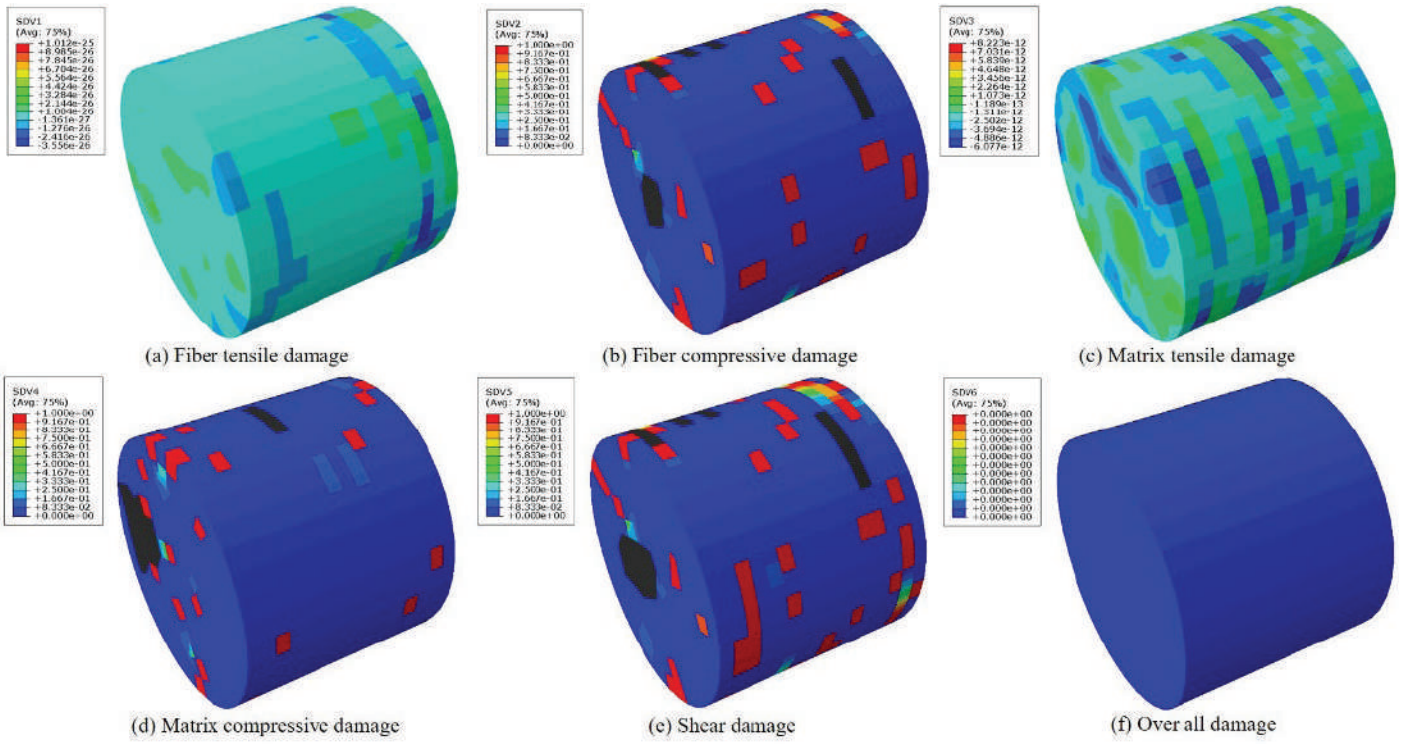

Figure 16. Damages obtained for cohesive interface model.

5. CONCLUSION

The behavior of CFRP composites under high strain rate deformation was investigated in this study using data from simulations conducted with various models. The simulation utilized a SHPB test set-up model with an initial velocity of 108 m/s in the striker. A user-defined Hashin damage model with a material degradation model VUMAT subroutine was employed to predict damages in the CFRP composite. The stress (σ)-strain(ε) plot shows that the percentage of obtained stress variations from the experiment reduces when the cohesive element is included in the model. Without cohesive, the stress values with respect to the experiment show a 2.98

% error, while with cohesive, the error is 2.54 %. At the same time, the cohesive parameters also influence the various damage parameters. Comparing stress-strain and stress-time behaviors, it was found that the cohesive interface model had the longest computing time, while the shell model required less time. A shell model is sufficient for non-essential structures to determine mechanical properties like strength. However, a cohesive interface model is necessary for essential structures such as satellites, turbine blades, and defense equipment where precision is crucial.

REFERENCES

1. Gauthier, L. Modelling of high velocity impact on composite materials for airframe structures application, 2010. (PhD Thesis).
2. Gavrus, A.; Bucur, F.; Rotariu, A. & Cananau, S. Mechanical behavior analysis of metallic materials using a Finite Element modeling of the SHPB test, a numerical calibration of the bar's elastic strains and an inverse analysis method. *Int. J. of Mater. Forming*, 2015, **8**, 567-579. doi: 10.1007/s12289-014-1180-0.
3. Gavrus, A.; Bucur, F.; Rotariu, A. & Cănănău, S. Analysis of metallic materials behavior during severe loadings using a FE modeling of the SHPB test based on a numerical calibration of elastic strains with respect to the raw measurements and on the inverse analysis principle. *Key Eng. Mater.*, 2013, **554**, 1133-1146. doi: 10.4028/www.scientific.net/KEM.554-557.1133
4. Jankowiak, T.; Rusinek, A. & Voyiadjis, G.Z. Modeling and design of SHPB to characterize brittle materials under compression for high strain rates. *Materials*, 2020, **13**(9), 2191. doi: 10.3390/ma13092191
5. Qu, K.; Wu, C.; Liu, J.; Yao, Y.; Deng, Y.; & Yi, C. Ballistic performance of multi-layered aluminium and UHMWPE fibre laminate targets subjected to hypervelocity impact by tungsten alloy ball. *Compos. Struct.,* 2015, 253, 112785. doi: 10.1016/j.compstruct.2020.112785
6. Hufner, D.R. & Hill, S.I. High strain rate testing and modeling of a woven E-glass–vinylester composite in dry and saturated conditions. *J. Compos. Mater.*, 2017, **51**(21), 3017-3039. doi: 10.1177/0021998316681185
7. Rathod, R.S.B.; Goel, M.D.; Chakraborty, T.; Matsagar, V.; Guégan, P. & Binetruy, C. Experimental and numerical investigations on dynamic behavior of CFRP laminates. *SN Appl. Sci*., 2019, 1, 1-10. doi: 10.1007/s42452-019-0732-9
8. Ren, L.; Yu, X.; Zheng, M.; Xue, Z.; Wu, B.; & He, Y. Evaluation of typical dynamic damage models used for UHPC based on SHPB technology. *Eng. Fracture Mechanics*, 2022, **269**, 108562. doi: 10.1016/j.engfracmech.2022.108562
9. Sawamura, Y.; Yamazaki, Y.; Yoneyama, S. & Koyanagi, J. Multi-scale numerical simulation of impact failure for cylindrical CFRP. *Adv. Compos. Mater.*, 2021, **30**(sup1), 19-38. doi: 10.1080/09243046.2020.1748789
10. Yerramalli, C.S.; Sumant, C.; Prusty, R.K. & Ray, B.C. Finite element modelling and experimentation of plain weave glass/epoxy composites under high strain-rate compression loading for estimation of Johnson-Cook model parameters. *Int. J Imp. Eng.*, 2022, **167**, 104262. doi: 10.1016/j.ijimpeng.2022.104262
11. Hinton, M.J.K.A.; Kaddour, A.S. & Soden, P.D. (Eds.). Failure criteria in fibre reinforced polymer composites: the world-wide failure exercise. Elsevier, 2004.
12. Kaddour, A.S. & Hinton, M.J. Challenging lessons from the second world-wide failure exercise (WWFE-II): Predicting failure in polymer composite laminates under 3-D states of stress. *In* 19th Int. Conference on Compos. Mater. (ICCM-19). Montreal, (2013).
13. Zheng, X. Nonlinear strain rate dependent composite model for explicit finite element analysis, 2006. (PhD Thesis).
14. Sellitto, A.; Saputo, S.; Di Caprio, F.; Riccio, A.; Russo, A. & Acanfora, V. Numerical–experimental correlation of impact-induced damages in CFRP laminates. *Appl. Sci.*, 2019, **9**(11), 2372. doi: 10.3390/app9112372
15. Chaurasia, B.K. Kumar, D. & Paswan, M.K. Experimental studies of failure in l-shaped carbon fiber-reinforced polymer composite under pullout and four-point bending. *In J. Inst. of Eng. (India): Series D*, 2022, 1-11. doi: 10.1007/s40033-022-00411-4
16. Riccio, A.; De Luca, A.; Di Felice, G. & Caputo, F. Modelling the simulation of impact induced damage onset and evolution in composites. *Compos. Part B: Eng.*, 2014, **66**, 340-347. doi: 10.1016/j.compositesb.2014.05.024
17. Aldoshan, A. & Khanna, S. Effect of relative density on the dynamic compressive behavior of carbon nanotube reinforced aluminum foam. *Mater. Sci. and Eng.: A*, 2017, **689**, 17-24. doi: 10.1016/j.msea.2017.01.100

ACKNOWLEDGMENT

We thank Central Research Facility NITK Surathkal for providing the high strain rate compressive test facilities.

CONTRIBUTORS

Dr Bipin Kumar Chaurasia is PhD Research scholar National Institute of Technology, Jamshedpur. He is involved in modelling of composite laminate based on damage model subjected to high strain loading, which induces stiffness reduction followed by non-linear progressive damage. He is also working toward fabrication of carbon fibre composites with optimum stacking which is intended to be used for improving material response under high velocity impact.
Contribution in the current study is conceptualization, methodology, software, validation, investigation writing – original draft.

Dr Deepak Kumar obtained his Ph.D. in Aerospace Engineering from Gyeongsang National University, South Korea. and working as an Assistant Professor in the Mechanical Engineering Department at the National Institute of Technology, Jamshedpur.

He is working in the field of damage mechanics of composite materials, nanocomposites, smart materials, product design, and development of biomaterials. Deepak also gained valuable experimental expertise in the areas of automated fiber placement technologies and composite bolted-joint mechanics. His latest research interests are the development of nanocomposites for development of super capacitor, energy devices and artificial tissues

Contribution in the current study is conceptualization, methodology, software, writing – review & editing, supervision.